

Theory of electrically controlled exhibition of circular Bragg phenomenon by an obliquely excited structurally chiral material

Akhlesh Lakhtakia¹

*Computational & Theoretical Materials Sciences Group (CATMAS)
Department of Engineering Science & Mechanics
Pennsylvania State University, University Park, PA 16802-6812, USA*

Juan Adrian Reyes²

*Instituto de Fisica
Universidad Nacional Autonoma de Mexico
Apartado Postal 20-364, C.P. 01000, Mexico D.F., Mexico*

Abstract: The boundary-value problem of the reflection and transmission of a plane wave due to a slab of an electro-optic structurally chiral material (SCM) is formulated in terms of a 4×4 matrix ordinary differential equation. The SCM slab can be locally endowed with one of 20 classes of point group symmetry, and is subjected to a dc voltage across its thickness. The enhancement (and, in some cases, the production) of the circular Bragg phenomenon (CBP) by the application of the dc voltage has either switching or circular-polarization-rejection applications in optics. The twin possibilities of thinner filters and electrical manipulation of the CBP, depending on the local crystallographic class as well as the constitutive parameters of the SCM, emerge.

Keywords: Circular Bragg phenomenon; Electro-optics; Pockels effect; Structural chirality;

1 Introduction

The Bragg phenomenon is exhibited by a slab of a material whose electromagnetic constitutive properties are periodically nonhomogeneous in the thickness direction. Its signature is very high reflectance in a certain wavelength-regime, provided the slab is thick enough to have a sufficiently large number of periods. This phenomenon is commonly exploited to make dielectric mirrors in optics [1, 2].

If the material is isotropic, no dependence of the Bragg phenomenon on the polarization state of a normally incident electromagnetic wave is evident. The material must be anisotropic for the Bragg phenomenon to discriminate between two mutually orthogonal polarization states [3].

Periodicity arises from structural chirality — i.e., a heliocidal variation of anisotropy along a fixed axis — in cholesteric liquid crystals [4, 5] and chiral sculptured thin films [6, 7], which exemplify structurally chiral materials (SCMs). Both types of SCMs are continuously nonhomogeneous in the thickness direction. SCMs can also be piecewise continuous, as proposed about 140 years ago by Reusch [8] and expanded upon recently by Hodgkinson *et al.* [9]. As the periodicity arises from structural chirality, incident electromagnetic plane waves of left- and right-circular polarization (LCP and RCP) states are reflected and transmitted differently

¹E-mail: akhlesh@psu.edu

²E-mail: adrian@fisica.unam.mx

in the Bragg wavelength–regime, and the Bragg phenomenon is then called the *circular* Bragg phenomenon (CBP). Exhibition of the CBP by cholesteric liquid crystals and chiral sculptured thin films underlies their use as circular–polarization rejection filters in optics [4, 6, 10].

Control of the CBP is very desirable for tuning the Bragg regime as well as for switching applications. One way would be to use SCMs that are electro–optic, because then the CBP could be electrically controlled. This possibility, also suggested by the fabrication of electro–optic Solč filters [11], was proposed and theoretically examined by us in a recent publication [12]. Therein, the SCM was assumed to possess locally a $\bar{4}2m$ point group symmetry for the exhibition of the Pockels effect [14], and the electromagnetic wave was taken to be normally incident on the SCM slab across whose thickness a low–frequency (or dc) electric field was supposed to be applied. The Pockels effect was found to enhance the CBP [12, 13], so much so that it could engender the CBP even if that phenomenon were to absent in the absence of a dc electric field.

In this paper, we take a comprehensive look at the planewave response characteristics of an electro–optic SCM slab. The electromagnetic plane wave can be either normally or obliquely incident. The SCM slab is locally endowed with one of 20 classes of point group symmetry [14] relevant to the excitation of the Pockels effect by a dc voltage applied across its thickness.

The organization of this paper is as follows: The theoretical formulation is presented in Section 2, beginning with the optical relative permittivity matrixes of a homogeneous electro–optic material and a SCM, going on to exploit the Oseen transformation to derive a 4×4 matrix ordinary differential equation for electromagnetic propagation in a SCM, then setting up a boundary–value problem to compute the reflectances and transmittances of a SCM slab, and finally discussing the salient features of axial propagation in a SCM. Section 3 is devoted to the presentation and discussion of numerical results. CBP enhancement by the application of the dc voltage is shown to have either switching or circular–polarization–rejection applications. The possibilities of thinner filters and electrical manipulation of the CBP, depending on the local crystallographic class as well as the constitutive parameters of the SCM, emerge from analysis for normal incidence.

A note about notation: Vectors are denoted in boldface; the cartesian unit vectors are represented by $\hat{\mathbf{u}}_x$, $\hat{\mathbf{u}}_y$, and $\hat{\mathbf{u}}_z$; symbols for column vectors and matrixes are decorated by an overbar; and an $\exp(-i\omega t)$ time–dependence is implicit with ω as the angular frequency.

2 Theoretical formulation

We are interested in the reflection and transmission of plane waves due to a SCM slab of thickness L . The axis of structural chirality of the SCM is designated as the z axis, and the SCM is subjected to a dc electric field $\mathbf{E}^{dc} = E_z^{dc} \hat{\mathbf{u}}_z$. The half–spaces $z \leq 0$ and $z \geq L$ are vacuous. An arbitrarily polarized plane wave is obliquely incident on the SCM from the half–space $z \leq 0$. As a result, reflected and transmitted plane waves exist in the half–spaces $z \leq 0$ and $z \geq L$, respectively. A boundary–value problem has to be solved in order to determine the reflection and transmission coefficients.

2.1 Pockels Effect

In order to delineate the electro–optic properties of the chosen SCM, let us first consider a (nondissipative) homogeneous dielectric material susceptible to the Pockels effect when subjected to a dc field \mathbf{E}^{dc} . The reciprocal of the optical relative permittivity matrix is usually

reported in the literature as [14]

$$\bar{\epsilon}_{PE}^{-1} = \begin{pmatrix} 1/\epsilon_1^{(0)} + \sum_{K=1}^3 r_{1K} E_K^{dc} & \sum_{K=1}^3 r_{6K} E_K^{dc} & \sum_{K=1}^3 r_{5K} E_K^{dc} \\ \sum_{K=1}^3 r_{6K} E_K^{dc} & 1/\epsilon_2^{(0)} + \sum_{K=1}^3 r_{2K} E_K^{dc} & \sum_{K=1}^3 r_{4K} E_K^{dc} \\ \sum_{K=1}^3 r_{5K} E_K^{dc} & \sum_{K=1}^3 r_{4K} E_K^{dc} & 1/\epsilon_3^{(0)} + \sum_{K=1}^3 r_{3K} E_K^{dc} \end{pmatrix} \quad (1)$$

in the principal Cartesian coordinate system (with axes labeled 1, 2, and 3) relevant to the crystallographic structure of the material [15, Table 7.1]. Here, $E_{1,2,3}^{dc}$ are the Cartesian components of the dc electric field, $\epsilon_{1,2,3}^{(0)}$ are the principal relative permittivity scalars in the optical regime, whereas r_{JK} (with $1 \leq J \leq 6$ and $1 \leq K \leq 3$) are the electro-optic coefficients in the traditional contracted or abbreviated notation for representing symmetric second-order tensors [14, 15].

This material can be isotropic, uniaxial, or biaxial, depending on the relative values of $\epsilon_1^{(0)}$, $\epsilon_2^{(0)}$, and $\epsilon_3^{(0)}$. Furthermore, this material may belong to one of 20 crystallographic classes of point group symmetry, in accordance with the relative values of the electro-optic coefficients r_{JK} [14, pp. 46–47].

Correct to the first order in the components of the dc electric field, we get the linear approximation

$$\bar{\epsilon}_{PE} \approx \begin{pmatrix} \epsilon_1^{(0)}(1 - \epsilon_1^{(0)} \sum_{K=1}^3 r_{1K} E_K^{dc}) & -\epsilon_1^{(0)} \epsilon_2^{(0)} \sum_{K=1}^3 r_{6K} E_K^{dc} & -\epsilon_1^{(0)} \epsilon_3^{(0)} \sum_{K=1}^3 r_{5K} E_K^{dc} \\ -\epsilon_2^{(0)} \epsilon_1^{(0)} \sum_{K=1}^3 r_{6K} E_K^{dc} & \epsilon_2^{(0)}(1 - \epsilon_2^{(0)} \sum_{K=1}^3 r_{2K} E_K^{dc}) & -\epsilon_2^{(0)} \epsilon_3^{(0)} \sum_{K=1}^3 r_{4K} E_K^{dc} \\ -\epsilon_3^{(0)} \epsilon_1^{(0)} \sum_{K=1}^3 r_{5K} E_K^{dc} & -\epsilon_3^{(0)} \epsilon_2^{(0)} \sum_{K=1}^3 r_{4K} E_K^{dc} & \epsilon_3^{(0)}(1 - \epsilon_3^{(0)} \sum_{K=1}^3 r_{3K} E_K^{dc}) \end{pmatrix} \quad (2)$$

from (1).

2.2 Structurally chiral material

As the electro-optic SCM has the z axis as its axis of chiral nonhomogeneity and is subjected to a dc electric field $\mathbf{E}^{dc} = E_z^{dc} \hat{\mathbf{u}}_z$, the optical relative permittivity matrix of this material may be stated as

$$\bar{\epsilon}^{SCM}(z) = \bar{S}_z \left(\frac{h\pi z}{\Omega} \right) \cdot \bar{R}_y(\chi) \cdot \bar{\epsilon}_{PE} \cdot \bar{R}_y(\chi) \cdot \bar{S}_z \left(-\frac{h\pi z}{\Omega} \right), \quad (3)$$

where $\bar{\epsilon}_{PE}$ is specified by (2). The tilt matrix

$$\bar{R}_y(\chi) = \begin{pmatrix} -\sin \chi & 0 & \cos \chi \\ 0 & -1 & 0 \\ \cos \chi & 0 & \sin \chi \end{pmatrix} \quad (4)$$

involves the angle $\chi \in [0, \pi/2]$ with respect to the x axis in the xz plane. The use of the rotation matrix

$$\bar{S}_z(\zeta) = \begin{pmatrix} \cos \zeta & -\sin \zeta & 0 \\ \sin \zeta & \cos \zeta & 0 \\ 0 & 0 & 1 \end{pmatrix} \quad (5)$$

in (3) involves the half-pitch Ω of the SCM along the z axis. In addition, the handedness parameter $h = 1$ for structural right-handedness and $h = -1$ for structural left-handedness.

Depending on the relationships between $\epsilon_1^{(0)}$, $\epsilon_2^{(0)}$, and $\epsilon_3^{(0)}$, a SCM may be classified as locally isotropic, locally uniaxial, or locally biaxial — the qualifier *local* referring to the crystallographic symmetry in any plane $z = \text{constant}$.

Furthermore, for the specific configuration of the dc electric field, we get

$$\left. \begin{aligned} E_1^{dc} &= E_z^{dc} \cos \chi \\ E_2^{dc} &= 0 \\ E_3^{dc} &= E_z^{dc} \sin \chi \end{aligned} \right\}. \quad (6)$$

2.3 Propagation in a SCM

The Maxwell curl postulates for the chosen SCM are given by

$$\left. \begin{aligned} \nabla \times \mathbf{E}(x, y, z) &= i\omega\mu_o\mathbf{H}(x, y, z) \\ \nabla \times \mathbf{H}(x, y, z) &= -i\omega\epsilon_o\bar{\epsilon}^{SCM}(z) \cdot \mathbf{E}(x, y, z) \\ 0 < z < L, \end{aligned} \right\}, \quad (7)$$

where ϵ_o and μ_o are the permittivity and the permeability of free space (i.e., vacuum).

As a plane wave is incident obliquely on the SCM, $\forall z$ we set [16, 17]

$$\left. \begin{aligned} \mathbf{E}(x, y, z) &= \mathbf{e}(z) \exp [i\kappa(x \cos \phi + y \sin \phi)] \\ \mathbf{H}(x, y, z) &= \mathbf{h}(z) \exp [i\kappa(x \cos \phi + y \sin \phi)] \end{aligned} \right\}, \quad (8)$$

where the wavenumber κ and the angle ϕ are determined by the incidence conditions. The essential part of the Maxwell curl postulates can then be stated in terms of the column vector [16, 18]

$$\bar{\psi}(z) = \begin{pmatrix} e_x(z) \\ e_y(z) \\ h_x(z) \\ h_y(z) \end{pmatrix}. \quad (9)$$

Inside the SCM, it is advantageous to exploit the Oseen transformation [16, 19] by defining the column vector

$$\bar{\psi}'(z) = \bar{M} \left(\frac{h\pi z}{\Omega} \right) \cdot \bar{\psi}(z), \quad (10)$$

where the unitary 4×4 matrix

$$\bar{M}(\zeta) = \begin{pmatrix} \cos \zeta & \sin \zeta & 0 & 0 \\ -\sin \zeta & \cos \zeta & 0 & 0 \\ 0 & 0 & \cos \zeta & \sin \zeta \\ 0 & 0 & -\sin \zeta & \cos \zeta \end{pmatrix}. \quad (11)$$

Following the procedure outlined by Lakhtakia and Weiglhofer [16], we have established that $\bar{\psi}'(z)$ satisfies the matrix ordinary differential equation

$$\frac{d}{dz} \bar{\psi}'(z) = i\bar{A}'(z) \cdot \bar{\psi}'(z), \quad 0 < z < L, \quad (12)$$

where

$$\begin{aligned}
\bar{A}'(z) = & \begin{pmatrix} 0 & -i\frac{h\pi}{\Omega} & 0 & \omega\mu_o \\ i\frac{h\pi}{\Omega} & 0 & -\omega\mu_o & 0 \\ 0 & -\omega\epsilon_o\epsilon_2^{(0)} & 0 & -i\frac{h\pi}{\Omega} \\ \omega\epsilon_o\epsilon_d & 0 & i\frac{h\pi}{\Omega} & 0 \end{pmatrix} + \kappa\delta_\epsilon \begin{pmatrix} \cos u & 0 & 0 & 0 \\ -\sin u & 0 & 0 & 0 \\ 0 & 0 & 0 & 0 \\ 0 & 0 & \sin u & \cos u \end{pmatrix} \\
& + \frac{\kappa^2}{\omega\epsilon_o} \frac{\epsilon_d}{\epsilon_1^{(0)}\epsilon_3^{(0)}} \left(1 + \frac{\alpha_2}{\epsilon_1^{(0)}\epsilon_3^{(0)}} \right) \begin{pmatrix} 0 & 0 & -\sin u \cos u & -\cos^2 u \\ 0 & 0 & \sin^2 u & \sin u \cos u \\ 0 & 0 & 0 & 0 \\ 0 & 0 & 0 & 0 \end{pmatrix} \\
& + \frac{\kappa^2}{\omega\mu_o} \begin{pmatrix} 0 & 0 & 0 & 0 \\ 0 & 0 & 0 & 0 \\ \sin u \cos u & \cos^2 u & 0 & 0 \\ -\sin^2 u & -\sin u \cos u & 0 & 0 \end{pmatrix} \\
& - \omega\epsilon_o \frac{\epsilon_2^{(0)}}{\epsilon_1^{(0)}} \begin{pmatrix} 0 & 0 & 0 & 0 \\ 0 & 0 & 0 & 0 \\ \epsilon_e + \epsilon_h & -\epsilon_m & 0 & 0 \\ \epsilon_l \cos \chi + (\epsilon_j + \epsilon_\ell) \frac{\sin 2\chi}{2} + \epsilon_k \sin \chi & -(\epsilon_e + \epsilon_h) & 0 & 0 \end{pmatrix} \\
& + \kappa \frac{\epsilon_2^{(0)}}{\epsilon_1^{(0)}\epsilon_3^{(0)}} \begin{pmatrix} -\frac{\alpha_1 \cos u}{\epsilon_1^{(0)}} & -(\epsilon_f + \epsilon_g) \cos u & 0 & 0 \\ \frac{\alpha_1 \sin u}{\epsilon_1^{(0)}} & (\epsilon_f + \epsilon_g) \sin u & 0 & 0 \\ 0 & 0 & (\epsilon_f + \epsilon_g) \sin u & (\epsilon_f + \epsilon_g) \cos u \\ 0 & 0 & -\frac{\alpha_1 \sin u}{\epsilon_1^{(0)}} & -\frac{\alpha_1 \cos u}{\epsilon_1^{(0)}} \end{pmatrix}, \quad (13)
\end{aligned}$$

$$\alpha_1 = \epsilon_1^{(0)} \epsilon_j \cos^2 \chi - \epsilon_3^{(0)} \epsilon_\ell \sin^2 \chi + \epsilon_1^{(0)} \epsilon_k \cos \chi - \epsilon_3^{(0)} \epsilon_i \sin \chi, \quad (14)$$

$$\alpha_2 = \left(\epsilon_1^{(0)} \epsilon_n + \epsilon_3^{(0)} \epsilon_p \right) \cos \chi + \left(\epsilon_1^{(0)} \epsilon_s + \epsilon_3^{(0)} \epsilon_q \right) \sin \chi, \quad (15)$$

$$\delta_\epsilon = \epsilon_d \sin 2\chi \frac{\left(\epsilon_1^{(0)} - \epsilon_3^{(0)} \right)}{2\epsilon_1^{(0)} \epsilon_3^{(0)}} \quad (16)$$

$$\epsilon_d = \frac{\epsilon_1^{(0)} \epsilon_3^{(0)}}{\epsilon_1^{(0)} \cos^2 \chi + \epsilon_3^{(0)} \sin^2 \chi}, \quad (17)$$

$$\epsilon_e = E_z^{dc} \epsilon_1^{(0)} \epsilon_d (r_{41} \cos^2 \chi - r_{63} \sin^2 \chi), \quad (18)$$

$$\epsilon_f = E_z^{dc} \epsilon_d \sin \chi \cos \chi (r_{41} \epsilon_3^{(0)} + r_{63} \epsilon_1^{(0)}), \quad (19)$$

$$\epsilon_g = E_z^{dc} \epsilon_d (r_{43} \epsilon_3^{(0)} \sin^2 \chi + r_{61} \epsilon_1^{(0)} \cos^2 \chi), \quad (20)$$

$$\epsilon_h = E_z^{dc} \epsilon_1^{(0)} \epsilon_d \sin \chi \cos \chi (r_{43} - r_{61}), \quad (21)$$

$$\epsilon_i = E_z^{dc} \frac{\epsilon_1^{(0)}}{\epsilon_2^{(0)}} \epsilon_d^2 (r_{31} \cos^2 \chi - r_{53} \sin^2 \chi), \quad (22)$$

$$\epsilon_j = E_z^{dc} \frac{\epsilon_1^{(0)}}{\epsilon_2^{(0)}} \epsilon_d^2 \sin \chi (r_{11} - r_{53}), \quad (23)$$

$$\epsilon_k = E_z^{dc} \frac{\epsilon_1^{(0)}}{\epsilon_2^{(0)}} \epsilon_d^2 (r_{13} \sin^2 \chi - r_{51} \cos^2 \chi), \quad (24)$$

$$\epsilon_\ell = E_z^{dc} \frac{\epsilon_1^{(0)}}{\epsilon_2^{(0)}} \epsilon_d^2 \cos \chi (r_{33} - r_{51}), \quad (25)$$

$$\epsilon_m = E_z^{dc} \epsilon_1^{(0)} \epsilon_2^{(0)} (r_{21} \cos \chi + r_{23} \sin \chi), \quad (26)$$

$$\epsilon_n = E_z^{dc} \epsilon_d (r_{53} \epsilon_3^{(0)} \sin^2 \chi + r_{11} \epsilon_1^{(0)} \cos^2 \chi), \quad (27)$$

$$\epsilon_p = E_z^{dc} \epsilon_d \sin^2 \chi (r_{31} \epsilon_3^{(0)} + r_{53} \epsilon_1^{(0)}), \quad (28)$$

$$\epsilon_q = E_z^{dc} \epsilon_d (r_{33} \epsilon_3^{(0)} \sin^2 \chi + r_{51} \epsilon_1^{(0)} \cos^2 \chi), \quad (29)$$

$$\epsilon_s = E_z^{dc} \epsilon_d \cos^2 \chi (r_{51} \epsilon_3^{(0)} + r_{13} \epsilon_1^{(0)}), \quad (30)$$

$$u = \frac{h\pi z}{\Omega} - \phi. \quad (31)$$

The matrix $\bar{A}'(z)$ is stated correct to the first order in E_z^{dc} .

By virtue of linearity, the solution of the 4×4 matrix ordinary differential equation oblique must be of the form

$$\bar{\psi}'(z_2) = \bar{U}'(z_2 - z_1) \cdot \bar{\psi}'(z_1), \quad (32)$$

whence

$$\begin{aligned}
\bar{\psi}(z_2) &= \bar{M}\left(-\frac{h\pi z_2}{\Omega}\right) \cdot \bar{U}'(z_2 - z_1) \cdot \bar{M}\left(\frac{h\pi z_1}{\Omega}\right) \cdot \bar{\psi}(z_1) \\
&\equiv \bar{U}(z_2 - z_1) \cdot \bar{\psi}(z_1), \\
&\quad 0 \leq z_\ell \leq L, \quad \ell = 1, 2.
\end{aligned} \tag{33}$$

There are at least two methods for calculating $\bar{U}'(z)$ [16, 20, 21], and we chose to implement the piecewise homogeneity approximation method [6, 21].

2.4 Reflection and transmission by a SCM slab

The incident plane wave is delineated by the phasors [6, 17]

$$\left. \begin{aligned}
\mathbf{e}_{inc}(z) &= \left(a_L \frac{is-\mathbf{p}_+}{\sqrt{2}} - a_R \frac{is+\mathbf{p}_+}{\sqrt{2}} \right) e^{ik_o z \cos \theta} \\
\mathbf{h}_{inc}(z) &= -i\eta_o^{-1} \left(a_L \frac{is-\mathbf{p}_+}{\sqrt{2}} + a_R \frac{is+\mathbf{p}_+}{\sqrt{2}} \right) e^{ik_o z \cos \theta}
\end{aligned} \right\}, \\
z &\leq 0,
\end{aligned} \tag{34}$$

where $\eta_o = \sqrt{\mu_o/\epsilon_o}$ is the intrinsic impedance of free space; a_L and a_R are the amplitudes of the LCP and RCP components, respectively; and the vectors

$$\mathbf{s} = -\hat{\mathbf{u}}_x \sin \phi + \hat{\mathbf{u}}_y \cos \phi, \tag{35}$$

$$\mathbf{p}_\pm = \mp (\hat{\mathbf{u}}_x \cos \phi + \hat{\mathbf{u}}_y \sin \phi) \cos \theta + \hat{\mathbf{u}}_z \sin \theta \tag{36}$$

are of unit magnitude. The propagation vector of the incident plane wave makes an angle $\theta \in [0, \pi/2)$ with respect to the $+z$ axis, and is inclined to the x axis in the xy plane by an angle $\psi \in [0, 2\pi]$; accordingly, the transverse wavenumber

$$\kappa = k_o \sin \theta, \tag{37}$$

where $k_o = \omega\sqrt{\epsilon_o\mu_o}$ is the wavenumber in free space. The free-space wavelength is denoted by $\lambda_o = 2\pi/k_o$.

The electromagnetic field phasors associated with the reflected and transmitted plane waves, respectively, are expressed by [6, 17]

$$\left. \begin{aligned}
\mathbf{e}_{ref}(z) &= \left(-r_L \frac{is-\mathbf{p}_-}{\sqrt{2}} + r_R \frac{is+\mathbf{p}_-}{\sqrt{2}} \right) e^{-ik_o z \cos \theta} \\
\mathbf{h}_{ref}(z) &= i\eta_o^{-1} \left(r_L \frac{is-\mathbf{p}_-}{\sqrt{2}} + r_R \frac{is+\mathbf{p}_-}{\sqrt{2}} \right) e^{-ik_o z \cos \theta}
\end{aligned} \right\}, \\
z &\leq 0,
\end{aligned} \tag{38}$$

and

$$\left. \begin{aligned}
\mathbf{e}_{tr}(z) &= \left(t_L \frac{is-\mathbf{p}_+}{\sqrt{2}} - t_R \frac{is+\mathbf{p}_+}{\sqrt{2}} \right) \\
&\quad \times e^{ik_o(z-L) \cos \theta} \\
\mathbf{h}_{tr}(z) &= -i\eta_o^{-1} \left(t_L \frac{is-\mathbf{p}_+}{\sqrt{2}} + t_R \frac{is+\mathbf{p}_+}{\sqrt{2}} \right) \\
&\quad \times e^{ik_o(z-L) \cos \theta}
\end{aligned} \right\}, \\
z &\geq L.
\end{aligned} \tag{39}$$

The amplitudes $r_{L,R}$ and $t_{L,R}$ indicate the as-yet unknown strengths of the LCP and RCP components of the reflected and transmitted plane waves, both of which are elliptically polarized in general.

As the tangential components of \mathbf{E} and \mathbf{H} must be continuous across the planes $z = 0$ and $z = L$, the boundary values $\bar{\psi}(0)$ and $\bar{\psi}(L)$ can be fixed by virtue of eq9.50–eq9.54. Hence,

$$\bar{\psi}(0) = \frac{1}{\sqrt{2}} \bar{K} \cdot \begin{bmatrix} i(a_L - a_R) \\ -(a_L + a_R) \\ -i(r_L - r_R) \\ r_L + r_R \end{bmatrix}, \quad (40)$$

and

$$\bar{\psi}(L) = \frac{1}{\sqrt{2}} \bar{K} \cdot \begin{bmatrix} i(t_L - t_R) \\ -(t_L + t_R) \\ 0 \\ 0 \end{bmatrix}, \quad (41)$$

where

$$\bar{K} = \begin{bmatrix} -\sin \phi & -\cos \phi \cos \theta & -\sin \phi & \cos \phi \cos \theta \\ \cos \phi & -\sin \phi \cos \theta & \cos \phi & \sin \phi \cos \theta \\ -\eta_o^{-1} \cos \phi \cos \theta & \eta_o^{-1} \sin \phi & \eta_o^{-1} \cos \phi \cos \theta & \eta_o^{-1} \sin \phi \\ -\eta_o^{-1} \sin \phi \cos \theta & -\eta_o^{-1} \cos \phi & \eta_o^{-1} \sin \phi \cos \theta & -\eta_o^{-1} \cos \phi \end{bmatrix}. \quad (42)$$

The reflection–transmission problem thus amounts to four simultaneous, linear algebraic equation stated in matrix form as

$$\begin{bmatrix} i(t_L - t_R) \\ -(t_L + t_R) \\ 0 \\ 0 \end{bmatrix} = \bar{K}^{-1} \cdot \bar{U}(L) \cdot \bar{K} \cdot \begin{bmatrix} i(a_L - a_R) \\ -(a_L + a_R) \\ -i(r_L - r_R) \\ r_L + r_R \end{bmatrix}. \quad (43)$$

This set of equations can be solved by standard matrix manipulations to compute the reflection and transmission coefficients.

It is usually convenient to define reflection and transmission coefficients. These appear as the elements of the 2×2 matrixes in the following relations:

$$\begin{bmatrix} r_L \\ r_R \end{bmatrix} = \begin{bmatrix} r_{LL} & r_{LR} \\ r_{RL} & r_{RR} \end{bmatrix} \begin{bmatrix} a_L \\ a_R \end{bmatrix}, \quad (44)$$

$$\begin{bmatrix} t_L \\ t_R \end{bmatrix} = \begin{bmatrix} t_{LL} & t_{LR} \\ t_{RL} & t_{RR} \end{bmatrix} \begin{bmatrix} a_L \\ a_R \end{bmatrix}. \quad (45)$$

Co-polarized coefficients have both subscripts identical, but cross-polarized coefficients do not. The square of the magnitude of a reflection or transmission coefficient is the corresponding reflectance or transmittance; thus, $R_{LR} = |r_{LR}|^2$ is the reflectance corresponding to the reflection coefficient r_{LR} , and so on. The principle of conservation of energy mandates the constraints

$$\left. \begin{aligned} R_{LL} + R_{RL} + T_{LL} + T_{RL} &\leq 1 \\ R_{RR} + R_{LR} + T_{RR} + T_{LR} &\leq 1 \end{aligned} \right\}, \quad (46)$$

the inequalities turning to equalities only in the absence of dissipation inside the SCM slab.

2.5 Normal incidence

For normal incidence, electromagnetic wave propagation in the SCM occurs parallel to the axis of structural chirality, and a special case amenable to algebraic analysis emerges [22]. Then $\kappa = 0$, and (12) simplifies to

$$\frac{d}{dz}\bar{\psi}'(z) = i\bar{A}'_{ax} \cdot \bar{\psi}'(z), \quad 0 < z < L, \quad (47)$$

wherein the matrix

$$\bar{A}'_{ax} = \begin{pmatrix} 0 & -i\frac{h\pi}{\Omega} & 0 & \omega\mu_o \\ i\frac{h\pi}{\Omega} & 0 & -\omega\mu_o & 0 \\ -\omega\epsilon_o\epsilon_E & -\omega\epsilon_o\epsilon_B & 0 & -i\frac{h\pi}{\Omega} \\ \omega\epsilon_o\epsilon_D & \omega\epsilon_o\epsilon_E & i\frac{h\pi}{\Omega} & 0 \end{pmatrix} \quad (48)$$

is independent of z , and

$$\epsilon_B = \epsilon_2^{(0)} - \frac{\epsilon_2^{(0)}}{\epsilon_1^{(0)}} \epsilon_m, \quad (49)$$

$$\epsilon_D = \epsilon_d - \frac{\epsilon_2^{(0)}}{\epsilon_1^{(0)}} \left[\epsilon_l \cos \chi + (\epsilon_j + \epsilon_l) \frac{\sin 2\chi}{2} + \epsilon_k \sin \chi \right], \quad (50)$$

$$\epsilon_E = \frac{\epsilon_2^{(0)}}{\epsilon_1^{(0)}} (\epsilon_e + \epsilon_h). \quad (51)$$

The solution of (47) therefore is straightforward:

$$\bar{U}'(z) = \exp [iz\bar{A}'_{ax}] \quad (52)$$

But an even more illuminating solution becomes available by further extending the Oseen transformation [23]. Let us define the column vector

$$\bar{\psi}''(z) = \bar{M}(h\xi) \cdot \bar{\psi}'(z), \quad (53)$$

where

$$\xi = \frac{1}{2} \tan^{-1} \left(\frac{2h\epsilon_E}{\epsilon_D - \epsilon_B} \right). \quad (54)$$

Then, (47) transforms to

$$\frac{d}{dz}\bar{\psi}''(z) = i\bar{A}''_{ax} \cdot \bar{\psi}''(z), \quad 0 < z < L, \quad (55)$$

where

$$\bar{A}''_{ax} = \begin{pmatrix} 0 & -i\frac{h\pi}{\Omega} & 0 & \omega\mu_o \\ i\frac{h\pi}{\Omega} & 0 & -\omega\mu_o & 0 \\ 0 & -\omega\epsilon_o\epsilon_{B\xi} & 0 & -i\frac{h\pi}{\Omega} \\ \omega\epsilon_o\epsilon_{D\xi} & 0 & i\frac{h\pi}{\Omega} & 0 \end{pmatrix}, \quad (56)$$

$$\epsilon_{B\xi} = \frac{1}{2} \left[\epsilon_B + \epsilon_D + \frac{(\epsilon_B - \epsilon_D)^2 + 4\epsilon_E^2}{\epsilon_B - \epsilon_D} \cos 2\xi \right], \quad (57)$$

$$\epsilon_{D\xi} = \frac{1}{2} \left[\epsilon_B + \epsilon_D - \frac{(\epsilon_B - \epsilon_D)^2 + 4\epsilon_E^2}{\epsilon_B - \epsilon_D} \cos 2\xi \right]. \quad (58)$$

The lower left quadrant of \bar{A}''_{ax} is antidiagonal; so is the lower left quadrant of \bar{A}'_{ax} when $E_z^{dc} = 0$. Thus, by comparison to extant results for non-electro-optic SCMs [6], we can state that the center-wavelength of the Bragg regime for normal incidence is

$$\lambda_o^{Br} = \Omega (\sqrt{\epsilon_{B\xi}} + \sqrt{\epsilon_{D\xi}}) \quad (59)$$

and the corresponding full-width-at-half-maximum (FWHM) bandwidth is

$$(\Delta\lambda_o)^{Br} = 2\Omega \left| \sqrt{\epsilon_{B\xi}} - \sqrt{\epsilon_{D\xi}} \right|, \quad (60)$$

with the assumption that dissipation in the SCM is negligibly small and dispersion in the constitutive properties can be ignored [24].

Correct to the second order in terms such as $r_{41}E_z^{dc}$, we get

$$\epsilon_{B\xi}^{1/2} \approx \sqrt{\epsilon_2^{(0)}} \left[1 - \frac{1}{2} \frac{\epsilon_m}{\epsilon_1^{(0)}} - \frac{1}{8} \left(\frac{\epsilon_m}{\epsilon_1^{(0)}} \right)^2 + \frac{1}{2} \left(\frac{\epsilon_2^{(0)}}{\epsilon_1^{(0)}} \right)^2 \frac{(\epsilon_e + \epsilon_h)^2}{\epsilon_2^{(0)}(\epsilon_2^{(0)} - \epsilon_d)} \right], \quad (61)$$

$$\epsilon_{D\xi}^{1/2} \approx \sqrt{\epsilon_d} \left[1 + \frac{1}{2} \frac{\epsilon_D - \epsilon_d}{\epsilon_d} - \frac{1}{8} \left(\frac{\epsilon_D - \epsilon_d}{\epsilon_d} \right)^2 - \frac{1}{2} \left(\frac{\epsilon_2^{(0)}}{\epsilon_1^{(0)}} \right)^2 \frac{(\epsilon_e + \epsilon_h)^2}{\epsilon_d(\epsilon_2^{(0)} - \epsilon_d)} \right], \quad (62)$$

which allows the delineation of the effect of the *local* crystallographic classification (as captured by the various electro-optic coefficients r_{JK}) on the extent of the Bragg regime. As an example, the foregoing expressions may be set down as

$$\epsilon_{B\xi}^{1/2} \approx \sqrt{\epsilon_2^{(0)}} \left[1 - \frac{1}{2} \epsilon_2^{(0)} E_z^{dc} r_{21} - \frac{1}{8} \left(\epsilon_2^{(0)} E_z^{dc} r_{21} \right)^2 + \frac{1}{2} \frac{\epsilon_2^{(0)}}{\epsilon_2^{(0)} - \epsilon_3^{(0)}} \left(\epsilon_3^{(0)} E_z^{dc} r_{41} \right)^2 \right], \quad (63)$$

$$\epsilon_{D\xi}^{1/2} \approx \sqrt{\epsilon_3^{(0)}} \left[1 - \frac{1}{2} \epsilon_3^{(0)} E_z^{dc} r_{31} - \frac{1}{8} \left(\epsilon_3^{(0)} E_z^{dc} r_{31} \right)^2 - \frac{1}{2} \frac{\epsilon_3^{(0)}}{\epsilon_2^{(0)} - \epsilon_3^{(0)}} \left(\epsilon_2^{(0)} E_z^{dc} r_{41} \right)^2 \right], \quad (64)$$

when $\chi = 0$. As another example, we get

$$\epsilon_{B\xi}^{1/2} \approx \sqrt{\epsilon_2^{(0)}} \left[1 - \frac{1}{2} \epsilon_2^{(0)} E_z^{dc} r_{23} - \frac{1}{8} \left(\epsilon_2^{(0)} E_z^{dc} r_{23} \right)^2 + \frac{1}{2} \frac{\epsilon_2^{(0)}}{\epsilon_2^{(0)} - \epsilon_1^{(0)}} \left(\epsilon_1^{(0)} E_z^{dc} r_{63} \right)^2 \right], \quad (65)$$

$$\epsilon_{D\xi}^{1/2} \approx \sqrt{\epsilon_1^{(0)}} \left[1 - \frac{1}{2} \epsilon_1^{(0)} E_z^{dc} r_{13} - \frac{1}{8} \left(\epsilon_1^{(0)} E_z^{dc} r_{13} \right)^2 - \frac{1}{2} \frac{\epsilon_1^{(0)}}{\epsilon_2^{(0)} - \epsilon_1^{(0)}} \left(\epsilon_1^{(0)} E_z^{dc} r_{63} \right)^2 \right], \quad (66)$$

when $\chi = \pi/2$.

Equations (65) and (66) do not hold for locally uniaxial SCMs (i.e., when $\epsilon_1^{(0)} = \epsilon_2^{(0)}$) [12]. Fresh analysis reveals

$$\begin{aligned} \epsilon_{B\xi}^{1/2} \approx & \sqrt{\epsilon_1^{(0)}} \left[1 + \frac{1}{4} \epsilon_1^{(0)} E_z^{dc} [\beta(r_{13} - r_{23}) - (r_{13} + r_{23})] \right. \\ & \left. - \frac{1}{32} \left\{ \epsilon_1^{(0)} E_z^{dc} [\beta(r_{13} - r_{23}) - (r_{13} + r_{23})] \right\}^2 \right], \end{aligned} \quad (67)$$

$$\begin{aligned} \epsilon_{D\xi}^{1/2} \approx & \sqrt{\epsilon_1^{(0)}} \left[1 - \frac{1}{4} \epsilon_1^{(0)} E_z^{dc} [\beta(r_{13} - r_{23}) + (r_{13} + r_{23})] \right. \\ & \left. - \frac{1}{32} \left\{ \epsilon_1^{(0)} E_z^{dc} [\beta(r_{13} - r_{23}) + (r_{13} + r_{23})] \right\}^2 \right], \end{aligned} \quad (68)$$

when $\chi = \pi/2$ and $\epsilon_2^{(0)} = \epsilon_1^{(0)}$; here,

$$\beta = \left[1 + \left(\frac{2r_{63}}{r_{13} - r_{23}} \right)^2 \right]^{1/2}. \quad (69)$$

Accordingly, the FWHM bandwidth of the Bragg regime turns out to be proportional to the magnitude of the dc electric field as per

$$(\Delta\lambda_o)^{Br} = 2\Omega(\epsilon_1^{(0)})^{3/2} \left| \beta E_z^{dc} (r_{13} - r_{23}) \left[1 + \frac{1}{4}\epsilon_1^{(0)} E_z^{dc} (r_{13} + r_{23}) \right] \right|. \quad (70)$$

Equation (70) indicates that the Bragg regime vanishes for normal incidence on a locally uniaxial, non-electro-optic SCM with $\chi = \pi/2$ [25], but can be generated by the appropriate application of a dc electric field if the SCM is electro-optic. This is the generalization of a result previously obtained for SCMs with local $\bar{4}2m$ point group symmetry [12]. Obviously, this conclusion may be exploited for optical switching applications for turning on or off a chosen circular polarization state.

The foregoing statements may be applied to locally biaxial SCMs as well in the following manner. Suppose that

$$\chi = \tan^{-1} \left[\left(\frac{\epsilon_1^{(0)}}{\epsilon_3^{(0)}} \right) \left(\frac{\epsilon_2^{(0)} - \epsilon_3^{(0)}}{\epsilon_1^{(0)} - \epsilon_2^{(0)}} \right) \right]^{1/2}; \quad (71)$$

then, $\epsilon_d = \epsilon_2^{(0)}$ by virtue of (17). For non-electro-optic SCMs, (71) defines the *pseudoisotropic point* [26, 27]: the Bragg regime for normal incidence vanishes, as may be seen by substituting (57) and (58) in (60), setting $E_z^{dc} = 0$ in the resulting expression, and making use of (71) thereafter. However, the Bragg regime can be restored by the application of E_z^{dc} , provided the SCM is electro-optic; the bandwidth of the Bragg regime can thus be electrically controlled. A general expression for $(\Delta\lambda_o)^{Br}$ at the pseudoisotropic point is far too cumbersome for reproduction here.

3 Numerical results and discussion

A Mathematica program was written to compute the reflectances and transmittances of a SCM slab of thickness L , on which an arbitrarily polarized plane wave is incident from the half-space $z < 0$ with an arbitrarily oriented wave vector. The principle of conservation of energy was verified to within $\pm 0.1\%$ error for all results presented in this section. All calculations were made for structurally right-handed SCMs.

3.1 Locally isotropic SCMs

Locally isotropic SCMs are characterized by $\epsilon_1^{(0)} = \epsilon_2^{(0)} = \epsilon_3^{(0)}$, and therefore cannot evince the circular Bragg phenomenon in the absence of a dc electric field. However, electro-optic materials of crystallographic classes $\bar{4}3m$ and 23 have $r_{41} = r_{52} = r_{63} \neq 0$ with all other $r_{JK} \equiv 0$ [28, pp. 170–176], and can therefore exhibit CBP when $E_z^{dc} \neq 0$ [2006].

Analysis of \bar{A}'_{ax} reveals that the application of E_z^{dc} would be infructuous towards the exhibition of the CBP for normal incidence (i.e., $\theta = 0^\circ$), if $\chi = 45^\circ$; but it would be most (and equally) effective for $\chi = 0^\circ$ and $\chi = 90^\circ$. The analytic continuability of $\bar{A}'(z)$ with respect to κ

suggests that the foregoing statement would be substantially true even for oblique incidence, at least for small and moderate values of θ ; and the validity of the suggestion was confirmed computationally.

Figures 1 and 2 help elucidate the effect of the dc electric field. The first figure shows the reflectance and transmittance spectrums for the incidence angle $\theta \in [0^\circ, 90^\circ)$ when $E_z^{dc} = 0$ and $\phi = 0^\circ$. The second figure has the same spectrums but when a dc voltage $V_{dc} = 8$ kV is applied across the planes $z = 0$ and $z = L$. The structurally right-handed SCM slab was taken to be 50Ω thick, $\Omega = 160$ nm, $\chi = 90^\circ$, and its local relative permittivity matrix and electro-optic parameters were chosen to be the same as of zinc telluride [28, p. 173].

In a ~ 40 -nm regime centered at $\lambda_o^{Br} = 956$ nm, R_{RR} is high and T_{RR} is low when $\theta = 0^\circ$, in Fig. 2. This is the Bragg regime, which blueshifts as $\cos\theta$ decreases from unity in magnitude. The Bragg regime is entirely absent in Fig. 1 when no dc voltage is applied. The Bragg regime is also absent in Fig. 2, even when the dc voltage is applied, for incident LCP plane waves. Clearly therefore, the Pockels effect has engendered the CBP in a SCM with a local crystallographic symmetry that is isotropic.

The cross-polarized reflectances and transmittances in the Bragg regime can be reduced by a variety of impedance-matching techniques [30], and thereafter the SCM slab can function as an electrically switchable circular-polarization rejection filter for incident plane waves of the same handedness as the SCM.

It is known from many studies on chiral sculptured thin films as well as cholesteric liquid crystals that the CBP first deepens and then saturates, as the normalized thickness L/Ω increases [6, 31]. The well-developed CBP manifests itself as a feature with a tall top-hat profile in the spectrum of R_{RR} (resp. R_{LL}) for normal and near-normal incidence on a structurally right-handed (resp. left-handed) slab. Further increase of thickness beyond a certain value of L/Ω is therefore infructuous. The same conclusion should hold true for an electro-optic SCM if E_z^{dc} were held fixed, and is indeed borne out in Fig. 3 by the plot of R_{RR} for a structurally right-handed SCM slab with other parameters the same as for the previous figure. This plot holds at the center-wavelength of the Bragg regime for normal incidence. Figure 3 also suggests that after a certain value, even an increase in E_z^{dc} for a fixed $L/2\Omega$ would lead to diminishing returns, if the objective is to maximize R_{RR} .

Electrical control of SCMs appears to require high dc voltages. These can be comparable with the half-wave voltages of electro-optic materials [32, p. 420], which are often in the 1–10 kV range. We must also note that the required magnitudes of E_z^{dc} are much smaller than the characteristic atomic electric field strength [14, p. 3]. Similarly high voltages are often applied to electro-optic films, albeit to create electric fields that are two orders-of-magnitude smaller than E_z^{dc} in Fig. 2 [33]. The possibility of electric breakdown exists, but it would significantly depend on the time that the dc voltage would be switched on for.

3.2 Locally uniaxial SCMs

Locally uniaxial SCMs are characterized by $\epsilon_1^{(0)} = \epsilon_2^{(0)} \neq \epsilon_3^{(0)}$. Crystals in 13 classes divided into the trigonal, tetragonal, and hexagonal families can exhibit the Pockels effect [14]. Lithium niobate and potassium dihydrogen phosphate are perhaps the most well-known uniaxial electro-optic materials, but a host of other materials with similar properties also exist [28, pp. 176–201].

Locally uniaxial SCMs should exhibit the CBP even in the absence of a dc electric field, and indeed they do, as is evident from Fig. 4 which shows the reflectance and transmittance spectrums for incidence angles $\theta \in [0^\circ, 90^\circ)$ and $\phi = 0^\circ$ when $E_z^{dc} = 0$. The chosen SCM has

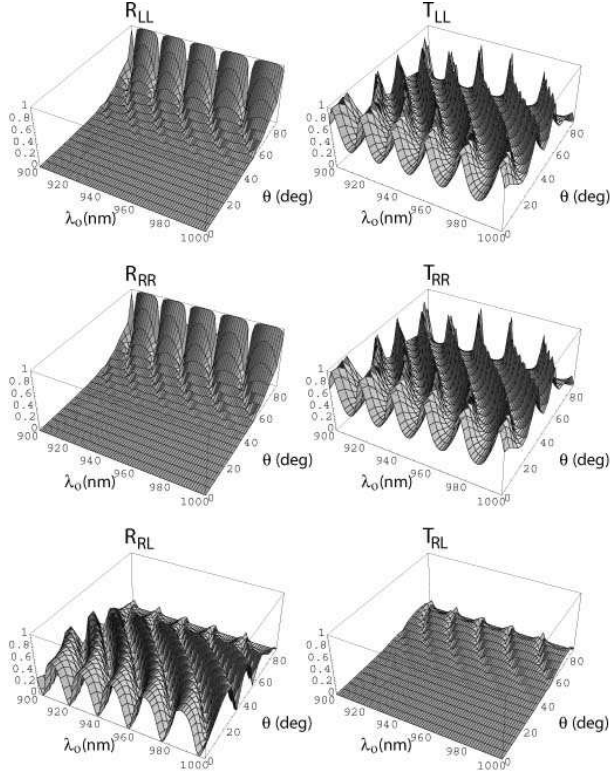


Figure 1: Reflectances and transmittances of a locally isotropic SCM slab of thickness $L = 50 \Omega$ as functions of the free-space wavelength λ_o and the incidence angle θ , when $E_z^{dc} = 0$ and $\phi = 0^\circ$. The local crystallographic class of the SCM is $\bar{4}3m$. Other parameters are: $\epsilon_1^{(0)} = \epsilon_2^{(0)} = \epsilon_3^{(0)} = 8.94$, $r_{41} = r_{52} = r_{63} = 4.04 \times 10^{-12} \text{ m V}^{-1}$, all other $r_{JK} = 0$, $h = 1$, $\Omega = 160 \text{ nm}$, and $\chi = 90^\circ$. These plots are the same as for $\chi = 0^\circ$. As $T_{LR} = T_{RL}$ and $R_{LR} = R_{RL}$ to numerical accuracy, the plots of T_{LR} and T_{RL} are not shown.

trigonal $3m$ as its local crystallographic class, with the values of the relative permittivity scalars and the electro-optic coefficients the same as for lithium niobate [28, p. 184]. The plots of R_{RR} and T_{RR} show the Bragg regime centered about $\lambda_o^{Br} = 648 \text{ nm}$ when $\theta = 0^\circ$, the Bragg regime exhibiting a blueshift with decrease of $\cos \theta$. The SCM slab is not very thick ($L = 20\Omega$); hence, the CBP is not fully developed [6, 31].

Figure 5 has the same reflectance and transmittance plots as the preceding figure, except that a dc voltage of 5 kV is applied across the SCM slab. The CBP in Fig. 5 is definitely enhanced in comparison to Fig. 4; calculated results not presented here indicate even a better developed CBP in the form of a broad top-hat profile of the R_{RR} -ridge for higher values of E_z^{dc} .

Thus, there are two ways to enhance the CBP for exploitation in circular-polarization rejection filters. The first is to use thicker SCM slabs, i.e., the ratios $L/2\Omega$ are large. The second is to use higher V_{dc} . The interplay between these two factors is indicated in Fig. 6, wherein R_{RR} for normal incidence and $\lambda_o = 648 \text{ nm}$ is plotted as a function of $L/2\Omega$ and E_z^{dc} . This figure clearly indicates that the exploitation of the Pockels effect will lead to thinner filters.

Qualitatively comparable results were obtained when the local crystallographic class was changed from trigonal $3m$ to any of the other 12 trigonal, tetragonal or hexagonal classes.

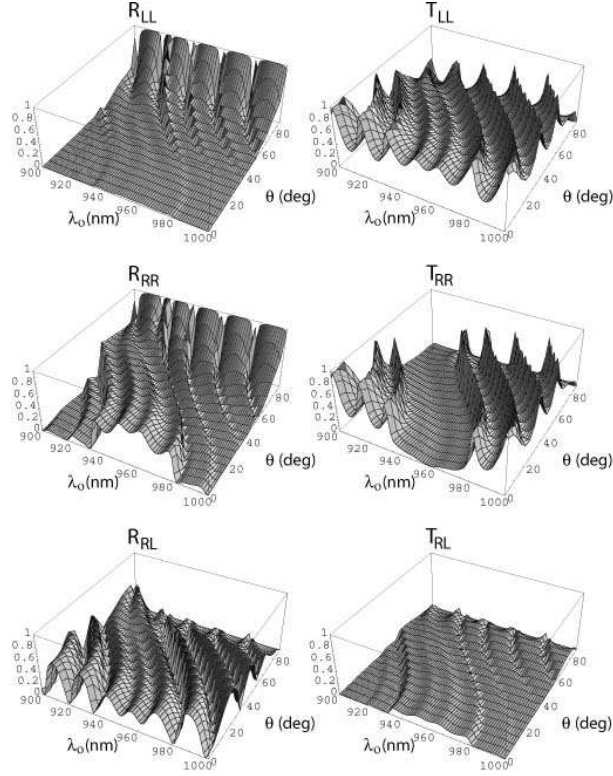


Figure 2: Same as Fig. 1, except that a dc voltage $V_{dc} = 8$ kV is applied between the planes $z = 0$ and $z = L$; thus, $E_z^{dc} = V_{dc}/L = 1$ GV m $^{-1}$. As the differences between T_{LR} and T_{RL} are very small, and $R_{LR} = R_{RL}$ to numerical accuracy, the plots of T_{LR} and T_{RL} are not shown. Note that $r_{41}E_z^{dc} = 0.00404$ is much smaller than $1/\epsilon_1^{(1)} = 0.1118$.

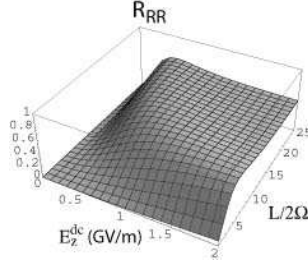


Figure 3: Reflectance R_{RR} of a locally isotropic SCM slab as a function of $L/2\Omega$ and E_z^{dc} . The local crystallographic class of the SCM is $\bar{4}3m$, with $\epsilon_1^{(0)} = \epsilon_2^{(0)} = \epsilon_3^{(0)} = 8.94$, $r_{41} = r_{52} = r_{63} = 4.04 \times 10^{-12}$ m V $^{-1}$, all other $r_{JK} = 0$, $h = 1$, $\Omega = 160$ nm, and $\chi = 90^\circ$. The angles of incidence $\theta = \phi = 0^\circ$, and the wavelength $\lambda_o = 956$ nm lies in the middle of the Bragg regime for normal incidence.

3.3 Locally biaxial SCMs

Locally biaxial SCMs are characterized by $\epsilon_1^{(0)} \neq \epsilon_2^{(0)} \neq \epsilon_3^{(0)}$. Crystals in 5 classes separated into the orthorhombic, monoclinic, and triclinic families can exhibit the Pockels effect [14]. Potassium niobate and sodium barium niobate are well-known biaxial electro-optic materials

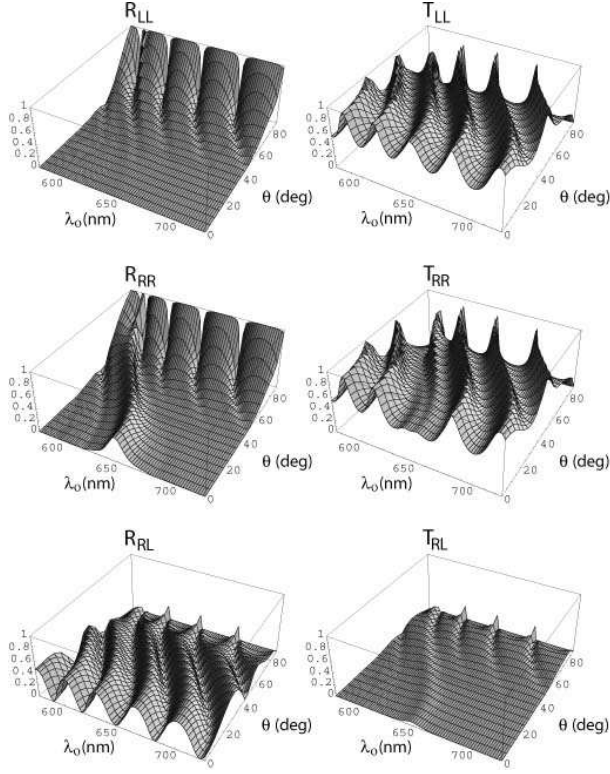


Figure 4: Reflectances and transmittances of a locally uniaxial SCM slab of thickness $L = 20\Omega$ as functions of the free-space wavelength λ_o and the incidence angle θ , when $E_z^{dc} = 0$ and $\phi = 0^\circ$. The local crystallographic class of the SCM is trigonal $3m$. Other parameters are: $\epsilon_1^{(0)} = \epsilon_2^{(0)} = 5.48, \epsilon_3^{(0)} = 5.04, r_{22} = -r_{12} = -r_{61} = 6.8 \times 10^{-12} \text{ m V}^{-1}, r_{13} = r_{23} = 9.6 \times 10^{-12} \text{ m V}^{-1}, r_{33} = 30.9 \times 10^{-12} \text{ m V}^{-1}, r_{42} = r_{51} = 32.6 \times 10^{-12} \text{ m V}^{-1}$, all other $r_{JK} = 0, h = 1, \Omega = 140 \text{ nm}$, and $\chi = 45^\circ$. As $T_{LR} = T_{RL}$ and $R_{LR} = R_{RL}$ to numerical accuracy, the plots of T_{LR} and T_{LR} are not shown.

[34, 35].

Just like their locally uniaxial counterparts, locally biaxial SCMs generally exhibit the CBP whether or not $E_z^{dc} = 0$. This is evident from Figs. 7 and 8 which show the reflectance and transmittance spectrums for incidence angles $\theta \in [0^\circ, 90^\circ)$ and $\phi = 0^\circ$ when $E_z^{dc} = 0$ and $E_z^{dc} = 0.67 \text{ GV m}^{-1}$, respectively. The chosen SCM has orthorhombic $mm2$ as its local crystallographic class, with the values of the relative permittivity scalars and the electro-optic coefficients the same as for potassium niobate [35]. The plots of R_{RR} and T_{RR} in both figures show the Bragg regime exhibiting a blueshift with decrease of $\cos \theta$. As the SCM slab is not very thick ($L = 20\Omega$), the CBP is not fully developed when $E_z^{dc} = 0$, but does exhibit the broad top-hat profile of the R_{RR} -ridge in Fig. 8 for $E_z^{dc} \neq 0$. Clearly then, the application of the dc voltage is efficacious in improving the CBP and confirms the conclusion made in Section 3.2 that it would lead to thinner filters.

When $E_z^{dc} = 0$, locally biaxial SCMs can possess a pseudoisotropic point defined via $\mathring{\text{dd}}3$, whose influence is best seen for normal incidence. For the relative permittivity scalars used to obtain the plots of Fig. 7, the pseudoisotropic point is identified by the value $\chi = 32.28^\circ$. Figures 9 and 10 show spectrums of the co-polarized reflectances R_{RR} and R_{LL} for the same

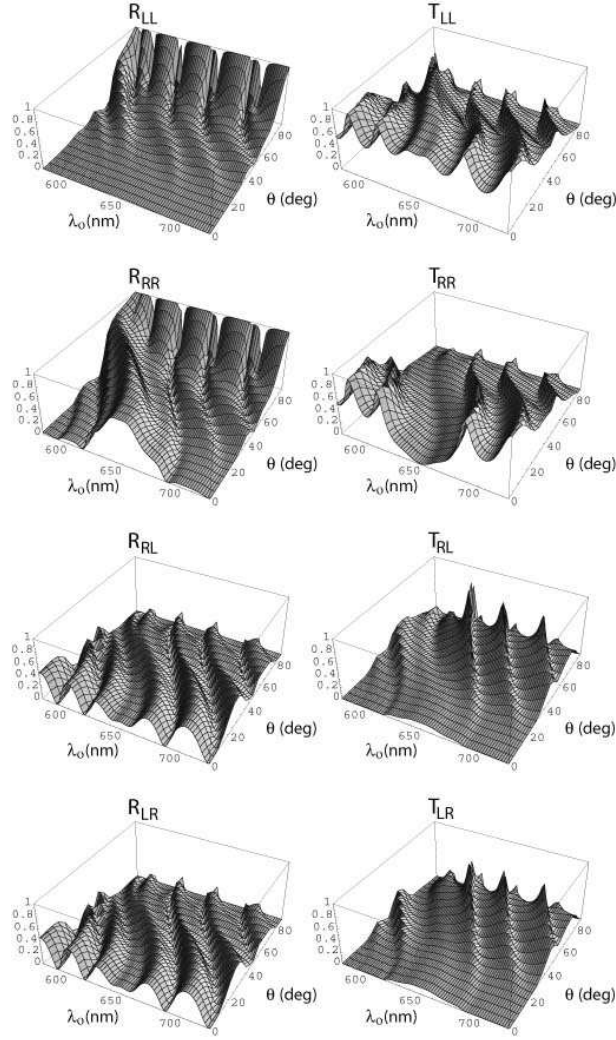


Figure 5: Same as Fig. 4, except that a dc voltage $V_{dc} = 5$ kV is applied between the planes $z = 0$ and $z = L$; thus, $E_z^{dc} = V_{dc}/L = 1.79$ GV m $^{-1}$.

parameters as for Figs. 7 and 8, respectively, except that $\chi = 32.28^\circ$. The Bragg regime is absent for θ less than at least 60° when $E_z^{dc} = 0$, but is restored in Fig. 10 by the application of a dc voltage.

3.4 Variation with ϕ

All plots shown heretofore are for $\phi = 0^\circ$. In general, there is some effect of ϕ on the reflectance and transmittance spectrums even in the absence of the Pockels effect, which can be attributed to the relative orientation of the incident electric field $\mathbf{e}_{inc}(0)$ with the principal components of the projection of $\bar{\epsilon}^{SCM}(0)$ on the plane $z = 0$ VL98. Similar variations are found when $E_z^{dc} \neq 0$, but do not affect the exhibition of the CBP — as may be gleaned from the plots of R_{RR} of a locally uniaxial SCM slab presented in Fig. 11.

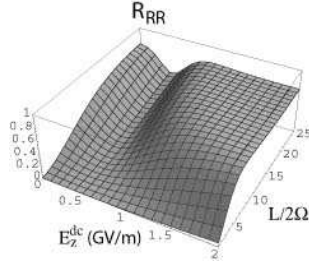


Figure 6: Reflectance R_{RR} of a locally uniaxial SCM slab as a function of $L/2\Omega$ and E_z^{dc} . The local crystallographic class of the SCM is trigonal $3m$, with $\epsilon_1^{(0)} = \epsilon_2^{(0)} = 5.48, \epsilon_3^{(0)} = 5.04, r_{22} = -r_{12} = -r_{61} = 6.8 \times 10^{-12} \text{ m V}^{-1}, r_{13} = r_{23} = 9.6 \times 10^{-12} \text{ m V}^{-1}, r_{33} = 30.9 \times 10^{-12} \text{ m V}^{-1}, r_{42} = r_{51} = 32.6 \times 10^{-12} \text{ m V}^{-1}$, all other $r_{JK} = 0, h = 1, \Omega = 140 \text{ nm}$, and $\chi = 45^\circ$. The angles of incidence $\theta = \phi = 0^\circ$, and the wavelength $\lambda_o = 648 \text{ nm}$ lies in the middle of the Bragg regime for normal incidence.

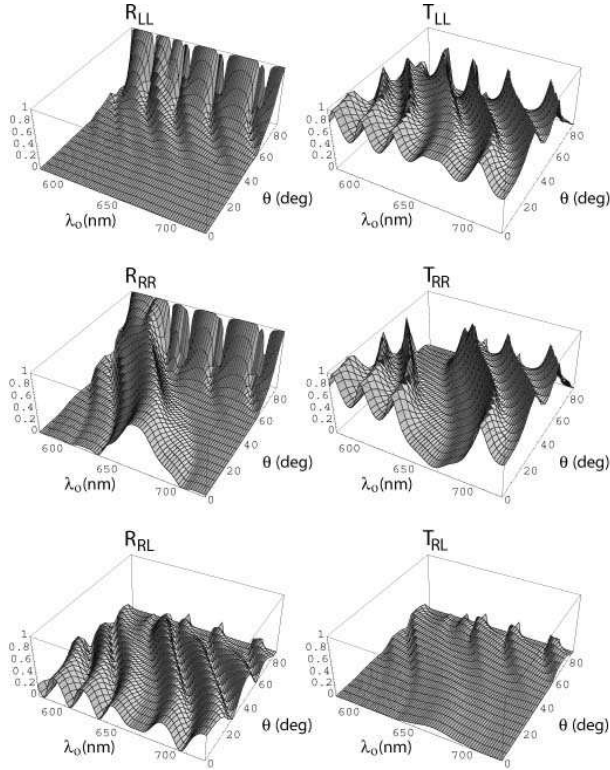


Figure 7: Reflectances and transmittances of a locally biaxial SCM slab of thickness $L = 20\Omega$ as functions of the free-space wavelength λ_o and the incidence angle θ , when $E_z^{dc} = 0$ and $\phi = 0^\circ$. The local crystallographic class of the SCM is orthorhombic $mm2$. Other parameters are: $\epsilon_1^{(0)} = 4.72, \epsilon_2^{(0)} = 5.20, \epsilon_3^{(0)} = 5.43, r_{13} = 34 \times 10^{-12} \text{ m V}^{-1}, r_{23} = 6 \times 10^{-12} \text{ m V}^{-1}, r_{33} = 63.4 \times 10^{-12} \text{ m V}^{-1}, r_{42} = 450 \times 10^{-12} \text{ m V}^{-1}, r_{51} = 120 \times 10^{-12} \text{ m V}^{-1}$, all other $r_{JK} = 0, h = 1, \Omega = 150 \text{ nm}$, and $\chi = 90^\circ$. As $T_{LR} = T_{RL}$ and $R_{LR} = R_{RL}$ to numerical accuracy, the plots of T_{LR} and T_{RL} are not shown.

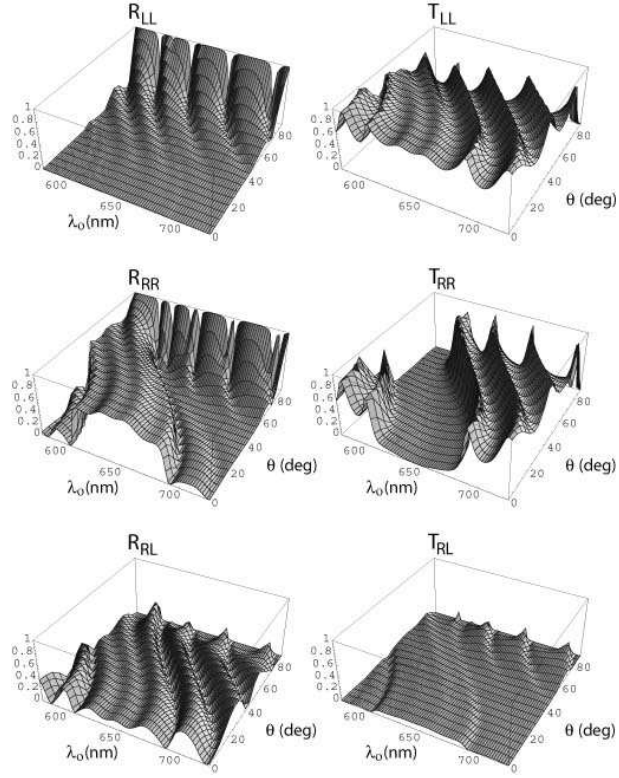


Figure 8: Same as Fig. 7, except that a dc voltage $V_{dc} = 2$ kV is applied between the planes $z = 0$ and $z = L$; thus, $E_z^{dc} = V_{dc}/L = 0.67$ GV m $^{-1}$.

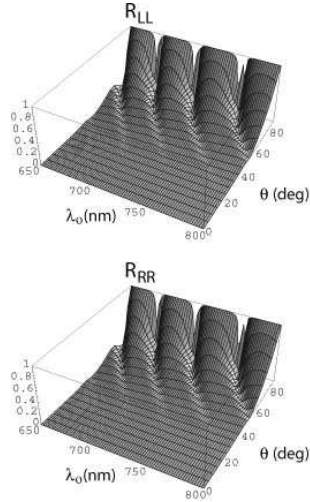


Figure 9: Co-polarized reflectances of a locally biaxial SCM slab when $V_{dc} = 0$. All parameters are the same as for Fig. 7, except that $\chi = 32.28^\circ$. Note the absence of the CBP at normal and near-normal incidences at the pseudoisotropic value chosen for χ .

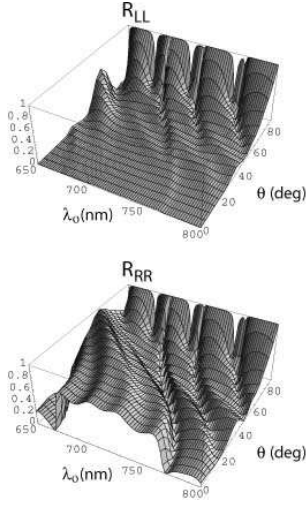


Figure 10: Co-polarized reflectances of a locally biaxial SCM slab when $V_{dc} = 2$ kV. All parameters are the same as for Fig. 9. Note the restoration of the CBP at normal and near-normal incidences at the pseudoisotropic value chosen for χ .

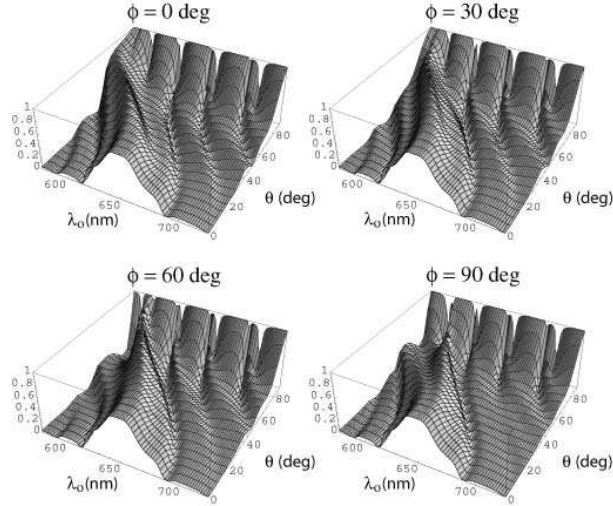


Figure 11: Co-polarized reflectance R_{RR} of a locally uniaxial SCM slab of thickness $L = 20 \Omega$ as a function of the free-space wavelength λ_o and the incidence angle θ , when $E_z^{dc} = 1.79$ GV m $^{-1}$, and $\phi = 0^\circ, 30^\circ, 60^\circ$, and 90° . The local crystallographic class of the SCM is trigonal $3m$. Other parameters are: $\epsilon_1^{(0)} = \epsilon_2^{(0)} = 5.48, \epsilon_3^{(0)} = 5.04, r_{22} = -r_{12} = -r_{61} = 6.8 \times 10^{-12}$ m V $^{-1}$, $r_{13} = r_{23} = 9.6 \times 10^{-12}$ m V $^{-1}$, $r_{33} = 30.9 \times 10^{-12}$ m V $^{-1}$, $r_{42} = r_{51} = 32.6 \times 10^{-12}$ m V $^{-1}$, all other $r_{JK} = 0$, $h = 1$, $\Omega = 140$ nm, and $\chi = 45^\circ$.

3.5 Electrical manipulation of the CBP

Several of the spectrums presented clearly show that the Bragg regime not only blueshifts but also narrows as $\cos \theta$ decreases, in line with previous reports on non-electro-optic SCMs [17]. Estimates of the blueshift and narrowing can be obtained from curve-fitting exercises [24]. The case of normal incidence ($\theta = 0^\circ$) therefore serves as a bellwether for oblique incidence;

the former is also significant in its own right, because it represents possibly the most useful configuration for optics. Therefore, as may be guessed from Section 2.5, it is fortuitous that closed-form expressions can be derived for important quantities for the normal-incidence case.

In the present context of the manipulation of the CBP by the application of a dc electric field, the two most important quantities are the center-wavelength λ_o^{Br} and the FWHM bandwidth $(\Delta\lambda_o)^{Br}$ of the Bragg regime for normal incidence, as defined in Br-def and dBr-def. Let us note that

$$\lambda_o^{Br} \Big|_{E_z^{dc}=0} = \Omega \left(\sqrt{\epsilon_2^{(0)}} + \sqrt{\epsilon_d} \right) \quad (72)$$

and

$$(\Delta\lambda_o)^{Br} \Big|_{E_z^{dc}=0} = 2\Omega \left| \sqrt{\epsilon_2^{(0)}} - \sqrt{\epsilon_d} \right|, \quad (73)$$

which expressions clearly indicate that, if the Pockels effect is not exploited, then

- (i) locally isotropic SCMs do not exhibit the CBP for all χ ,
- (ii) locally uniaxial SCMs do not exhibit the CBP if $\chi = 90^\circ$, and
- (iii) locally biaxial SCMs do not exhibit the CBP if χ satisfies the pseudoisotropic condition dd3.

Against this backdrop, the role of the Pockels effect on the CBP can be assessed analytically.

Table 1 shows the dependencies of ϵ_E , ϵ_B , and ϵ_D on χ , for all 20 local crystallographic classes. In addition, ϵ_E may be a function of r_{41} , r_{43} , r_{61} , and r_{63} ; ϵ_B of r_{21} , and r_{23} ; and ϵ_D of r_{11} , r_{13} , r_{31} , r_{33} , r_{51} , and r_{53} . Finally, ϵ_E , ϵ_B , and ϵ_D vary linearly with E_z^{dc} . To second order in E_z^{dc} then,

$$\begin{aligned} \sqrt{\epsilon_{B\xi}} \approx & \sqrt{\epsilon_2^{(0)}} + f_1(r_{21}, r_{23}, \chi) E_z^{dc} \\ & + f_2(r_{21}, r_{23}, r_{41}, r_{43}, r_{61}, r_{63}, \chi) \left(E_z^{dc} \right)^2 \end{aligned} \quad (74)$$

and

$$\begin{aligned} \sqrt{\epsilon_{D\xi}} \approx & \sqrt{\epsilon_d} + f_3(r_{11}, r_{13}, r_{31}, r_{33}, r_{51}, r_{53}, \chi) E_z^{dc} \\ & + f_4(r_{11}, r_{13}, r_{31}, r_{33}, r_{41}, r_{43}, r_{51}, r_{53}, r_{61}, r_{63}, \chi) \\ & \times \left(E_z^{dc} \right)^2, \end{aligned} \quad (75)$$

where f_1 to f_4 are functions of the identified electro-optic coefficients and the tilt angle. Substitution of the foregoing expressions in Br-def then leads to the following five statements:

- A. For both classes of locally isotropic SCMs, the shift of λ_o^{Br} does not depend on E_z^{dc} but on $\left(E_z^{dc} \right)^2$.
- B. For four classes of locally uniaxial SCMs, the shift of λ_o^{Br} does not depend on E_z^{dc} but on $\left(E_z^{dc} \right)^2$. The four classes are tetragonal 422, tetragonal $\bar{4}2m$, hexagonal 622, and hexagonal $\bar{6}m2$.

- C. For the remaining nine classes of locally uniaxial SCMs, the shift of λ_o^{Br} depends on both E_z^{dc} and $(E_z^{dc})^2$.
- D. For three classes of locally biaxial SCMs, the shift of λ_o^{Br} does not depend on E_z^{dc} but on $(E_z^{dc})^2$. The four classes are orthorhombic 222 , monoclinic 2 , and monoclinic m .
- E. For the remaining two classes of locally biaxial SCMs, the shift of λ_o^{Br} depends on both E_z^{dc} and $(E_z^{dc})^2$.

Statements A to E for a *shift* in the center–wavelength λ_o^{Br} upon the application of a dc voltage also hold true for the concurrent *change* in the FWHM bandwidth $(\Delta\lambda_o)^{Br}$.

Therefore, the center–wavelengths of the Bragg regimes of SCMs of 11 local crystallographic classes will *shift*, and the FWHM bandwidths of the same will *change*, on the application of moderate dc voltages; whereas those of SCMs of the remaining nine local crystallographic classes will require the application of higher dc voltages to shift. Furthermore, the Bragg regimes will either redshift or blueshift, depending on the sign of E_z^{dc} , for the 11 local crystallographic classes; but the shifts of the Bragg regimes will be insensitive to the sign of E_z^{dc} , for the remaining nine local crystallographic classes. These conclusions were verified by comparing the Bragg–regime spectrums for trigonal $3m$, orthorhombic $mm2$, and tetragonal $\bar{4}2m$ (not shown here) classes.

The effect of the tilt angle χ on the FWHM bandwidth of the Bragg regime for normal incidence is quite modified by the application of E_z^{dc} . Statements (i) to (iii) are replaced as follows: When $E_z^{dc} \neq 0$,

- I. locally isotropic SCMs do not exhibit the CBP only if $\chi = 45^\circ$;
- II. locally uniaxial SCMs do not exhibit the CBP if $\chi = 90^\circ$, provided the local crystallographic class is neither tetragonal $\bar{4}$ nor tetragonal $\bar{4}2m$; and
- III. locally biaxial SCMs exhibit the CBP even if χ satisfies the pseudoisotropic condition $\bar{d}d3$.

When $\chi = 0^\circ$, the center–wavelength of the Bragg regime does not shift for the following local crystallographic classes: tetragonal $4mm$, hexagonal $6mm$, hexagonal $\bar{6}m2$, trigonal $3m$, and orthogonal $mm2$. Likewise, when $\chi = 90^\circ$, the center–wavelength of the Bragg regime does not shift for the following local crystallographic classes: tetragonal 422 , hexagonal 622 , hexagonal $\bar{6}$, hexagonal $\bar{6}m2$, and trigonal 32 .

4 Concluding remarks

A comprehensive treatment of the response characteristics of a slab of an electro–optic structurally chiral medium to normally as well as obliquely incident plane waves was undertaken in this paper. The SCM slab is endowed with one of 20 classes of point group symmetry, and is subjected to a dc voltage across its thickness. The boundary–value problem was cast in the form of a 4×4 matrix ordinary differential equation, whose solution yielded the reflectances and transmittances of the SCM slab. The improvement — and, in some instances, the creation — of the circular Bragg phenomenon by the application of the dc voltage was theoretically demonstrated and predicted to have either switching or circular–polarization–rejection applications in optics. The possibility of thinner filters and electrical manipulation of the CBP, depending on the local crystallographic class as well as the constitutive parameters of the SCM, were established. This comprehensive study is expected to provide impetus to experimental research, possibly on ambichiral versions of SCMs [37].

Before concluding, let us contextualize the foregoing work in optics today. SCMs can be considered to be one-dimensional photonic crystals (PCs). PCs have by now reached a mature stage of development, with their optical response characteristics well-understood and with many actual and potential applications [38, 39]. A recent trend concerns tunable or active PCs, whose optical response characteristics can change by means of some external agent. One way is to change their structural properties, for instance, by the application of mechanical stress [40, 41]. Another way is to change their electromagnetic constitutive parameters, e.g., by incorporating the magnetically tunable ferroelectric and ferromagnetic materials [42, 43, 44] or by infiltrating a PC with the electrically controllable liquid crystals [45, 46]. We have shown here that the Pockels effect can be similarly exploited.

Acknowledgments. We thank Partha P. Banerjee (University of Dayton, OH, USA) and Venkat Gopalan (Pennsylvania State University, PA, USA) for references on electro-optic materials.

References

- [1] H.A. Macleod, *Thin-Film Optical Filters*, 3rd ed., Institute of Physics Publishing, Bristol, United Kingdom, 2001.
- [2] P.W. Baumeister, *Optical Coating Technology*, SPIE Press, Bellingham, WA, USA, 2005.
- [3] I.J. Hodgkinson, Q.h. Wu, *Birefringent Thin Films and Polarizing Elements* World Scientific, Singapore, 1997.
- [4] P.G. de Gennes, J. Prost, *The Physics of Liquid Crystals*, 2nd ed., Clarendon Press, Oxford, UK, 1993, Chap. 6.
- [5] C.G. Avendaño, S. Ponti, J.A. Reyes, C. Oldano, *J. Phys. A: Math. Gen.* **38**, 8821 (2005).
- [6] A. Lakhtakia, R. Messier, *Sculptured Thin Films: Nanoengineered Morphology and Optics*, SPIE Press, Bellingham, WA, USA, 2005, Chap. 9.
- [7] K. Robbie, M.J. Brett, A. Lakhtakia, Chiral sculptured thin films, *Nature* 384 (1996) 616.
- [8] E. Reusch, Untersuchung über Glimmercombinationen, *Ann. Phys. Chem. Lpz.* 138 (1869) 628–638.
- [9] I.J. Hodgkinson, A. Lakhtakia, Q.h. Wu, L. De Silva, M.W. McCall, Ambichiral, equichiral and finely chiral layered structures, *Opt. Commun.* 239 (2004) 353–358.
- [10] S.D. Jacobs (ed.), *Selected Papers on Liquid Crystals for Optics*, SPIE Optical Engineering Press, Bellingham, WA, USA, 1992.
- [11] D.A. Pinnow, R.L. Abrams, J.F. Lotspeich, D.M. Henderson, T.K. Plant, R.R. Stephens, C.M. Walker, An electro-optic tunable filter, *Appl. Phys. Lett.* 34 (1979) 391–393.
- [12] J.A. Reyes, A. Lakhtakia, Electrically controlled optical bandgap in a structurally chiral material, *Opt Commun.* 259 (2006) 164–173.

- [13] J.A. Reyes, A. Lakhtakia, Electrically controlled reflection and transmission of obliquely incident light by structurally chiral materials, *Opt. Commun.* xxx (2006) xxx–xxx (doi:10.1016/j.optcom.2006.05.037).
- [14] R.W. Boyd, *Nonlinear Optics*, Academic Press, London, UK, 1992, Chap. 10.
- [15] B.A. Auld, *Acoustic Fields and Waves in Solids*, Vol. 1, Krieger, Malabar, FL, USA, 1990.
- [16] A. Lakhtakia, W.S. Weiglhofer, Further results on light propagation in helicoidal bianisotropic mediums: Oblique propagation, *Proc. R. Soc. Lond. A* 453 (1997) 93–105; correction: 454 (1998) 3275.
- [17] V.C. Venugopal, A. Lakhtakia, Electromagnetic plane-wave response characteristics of non-axially excited slabs of dielectric thin-film helicoidal bianisotropic mediums, *Proc. R. Soc. Lond. A* 456 (2000) 125–161.
- [18] N. Marcuvitz, J. Schwinger, On the representation of the electric and magnetic fields produced by currents and discontinuities in wave guides. I, *J. Appl. Phys.* 22 (1951) 806–819.
- [19] C.W. Oseen, The theory of liquid crystals, *J. Chem. Soc. Faraday Trans. II* 29 (1933) 883–899.
- [20] M. Schubert, C.M. Herzinger, Ellipsometry on anisotropic materials: Bragg conditions and phonons in dielectric helical thin films, *Phys. Stat. Sol. (a)* 188 (2001) 1563–1575.
- [21] J.A. Polo, Jr., A. Lakhtakia, Comparison of two methods for oblique propagation in helicoidal bianisotropic mediums, *Opt. Commun.* 230 (2004) 369–386.
- [22] A. Lakhtakia, W.S. Weiglhofer, On light propagation in helicoidal bianisotropic mediums, *Proc. R. Soc. Lond. A* 448 (1995) 419–437; correction: **454** (1998) 3275.
- [23] A. Lakhtakia, Generalized Oseen transformation for and enhancement of Bragg characteristics of electro-optic structurally chiral materials, *Opt. Commun.* 261 (2006) 213–217.
- [24] V.C. Venugopal, A. Lakhtakia, On absorption by non-axially excited slabs of dielectric thin-film helicoidal bianisotropic mediums, *Eur. Phys. J. Appl. Phys.* 10 (2000) 173–184.
- [25] V.C. Venugopal, A. Lakhtakia, Second harmonic emission from an axially excited slab of a dielectric thin-film helicoidal bianisotropic medium, *Proc. R. Soc. Lond. A* 454 (1998) 1535–1571; correction: 455 (1999) 4383.
- [26] I. Abdulhalim, Point of ultra-sensitivity to perturbations for axial propagation in helicoidal bianisotropic structures, *Europhys. Lett.* 48 (1999) 177–181.
- [27] A. Lakhtakia, W.S. Weiglhofer, A comparative study of planewave propagation in helicoidal bianisotropic mediums and isotropic chiral mediums, *J. Opt. A: Pure Appl. Opt.* 2 (2000) 107–111.
- [28] W.R. Cook Jr., Electrooptic coefficients, In: D.F. Nelson (ed.), *Landolt–Bornstein Volume III/30A*, Springer, Berlin, Germany, 1996.
- [29] A. Lakhtakia, Electrically switchable exhibition of circular Bragg phenomenon by an isotropic slab, *Microw. Opt. Technol. Lett.* 48 (2006) 2148–2153.

- [30] I.J. Hodgkinson, Q.h. Wu, M. Arnold, M.W. McCall, A. Lakhtakia, Chiral mirror and optical resonator designs for circularly polarized light: suppression of cross-polarized reflectances and transmittances, *Opt. Commun.* 210 (2002) 202–211.
- [31] W.D. St. John, W.J. Fritz, Z.J. Lu, D.-K. Yan, Bragg reflection from cholesteric liquid crystals, *Phys. Rev. E* 51 (1995) 1191–1198.
- [32] A. Yariv and P. Yeh, *Photonics: Optical Electronics in Modern Communications*, 6th ed., Oxford University Press, New York, NY, USA, 2007.
- [33] D.A. Scrymgeour, Y. Barad, V. Gopalan, K.T. Gahagan, Q. Jia, T.E. Mitchell, J.M. Robinson, Large-angle electro-optic laser scanner on LiTaO₃ fabricated by *in situ* monitoring of ferroelectric-domain micropatterning. *Appl. Opt.* 40 (2001) 6236–6241.
- [34] S. Singh, D.A. Draeger, J.E. Geusic, Optical and ferroelectric properties of barium sodium nitrate, *Phys. Rev. B* 2 (1970) 2709–2724.
- [35] M. Zgonik, R. Schlessler, I. Biaggio, E. Volt, J. Tscherry, P. Günter, Material constants of KNbO₃ relevant for electro- and acousto-optics, *J. Appl. Phys.* 74 (1993) 1287–1297.
- [36] V.C. Venugopal, A. Lakhtakia, On optical rotation and ellipticity transformation by axially excited slabs of dielectric thin-film helicoidal bianisotropic mediums (TFHBMs), *Int. J. Appl. Electromag. Mech.* 9 (1998) 201–210.
- [37] A. Lakhtakia, Ambichiral, electro-optic, circular-polarization rejection filters: theory, *Phys. Lett. A* 354 (2006) 330–334.
- [38] J.D. Joannopoulos, R.D. Meade, J.N. Winn, *Photonic Crystals*, Princeton University Press, Princeton, NJ, USA, 1995.
- [39] K. Sakoda, *Optical Properties of Photonic Crystals*, Springer, Heidelberg, Germany, 2001.
- [40] K. Yoshino, Y. Kawagishi, M. Ozaki, A. Kose, Mechanical tuning of the optical properties of plastic opal as a photonic crystal, *Jpn. J. Appl. Phys.* 38 (1999) L786–L788.
- [41] S. Kim, V. Gopalan, Strain-tunable photonic band gap crystals, *Appl. Phys. Lett.* 78 (2001) 3015–3017.
- [42] A. Figotin, Y. A. Godin, I. Vitebski, Two-dimensional tunable photonic crystals, *Phys. Rev. B* 57 (1998) 2841–2848.
- [43] J. Zhou, C.Q. Sun, K. Pita, Y.L. Lam, Y. Zhou, S.L. Ng, C.H. Kam, L.T. Li, Z.L. Gui, Thermally tuning of the photonic band gap of SiO₂ colloid-crystal infilled with ferroelectric BaTiO₃, *Appl. Phys. Lett.* 78 (2001) 661–663.
- [44] I.L. Lyubchanskii, N.N. Dadoenkova, M.I. Lyubchanskii, E.A. Shapovalov, A. Lakhtakia, Th. Rasing, One-dimensional bigyrotropic magnetic photonic crystals, *Appl. Phys. Lett.* 85 (2004) 5932–5934.
- [45] D.N. Chigrin, A.V. Lavrinenko, D.A. Yarotsky, S.V. Gaponenko, Observation of total omnidirectional reflection from a one-dimensional dielectric lattice, *Appl. Phys. A* 68 (1999) 25–28.

- [46] P. Halevi, J.A. Reyes–Avenidaño, J.A. Reyes–Cervantes, Electrically tuned phase transition and band structure in a liquid–crystal–infilled photonic crystal, *Phys. Rev. E* 73 (2006) 040701.

Table 1 Dependencies of ϵ_E , ϵ_B , and ϵ_D on χ , for the 20 classes of local crystallographic symmetry. The coefficients a_1 to a_{16} depend on various electro-optic coefficients.

local crystallographic class	$\epsilon_E \epsilon_d$	$\epsilon_B - \epsilon_2^{(0)}$	$(\epsilon_D - \epsilon_d)\epsilon_d^2$
cubic 23	$\cos(2\chi)$	0	0
cubic $\bar{4}3m$	$\cos(2\chi)$	0	0
tetragonal 4	$\cos^2 \chi$	$\sin \chi$	$[a_{10} + a_{11} \cos(2\chi)] \sin \chi$
tetragonal $4mm$	0	$\sin \chi$	$[a_{10} + a_{11} \cos(2\chi)] \sin \chi$
tetragonal 422	$\cos^2 \chi$	0	0
tetragonal $\bar{4}$	$a_1 + a_2 \cos(2\chi)$	$\sin \chi$	$[a_{13} + a_{14} \cos(2\chi)] \sin \chi$
tetragonal $\bar{4}2m$	$a_1 + a_2 \cos(2\chi)$	0	0
hexagonal 6	$\cos^2 \chi$	$\sin \chi$	$[a_{10} + a_{11} \cos(2\chi)] \sin \chi$
hexagonal $6mm$	0	$\sin \chi$	$[a_{10} + a_{11} \cos(2\chi)] \sin \chi$
hexagonal 622	$\cos^2 \chi$	0	0
hexagonal $\bar{6}$	$\sin(2\chi)$	$\cos \chi$	$\cos \chi \sin^2 \chi$
hexagonal $\bar{6}m2$	$\sin(2\chi)$	0	0
trigonal 3	$a_4 \cos \chi + a_5 \sin \chi$	$a_6 \cos \chi + a_7 \sin \chi$	$[a_{10} + a_{11} \cos(2\chi) + a_{12} \sin(2\chi)] \sin \chi$
trigonal $3m$	$\sin(2\chi)$	$\sin \chi$	$[a_{10} + a_{11} \cos(2\chi)] \sin \chi$
trigonal 32	$\cos^2 \chi$	$\cos \chi$	$\cos \chi \sin^2 \chi$
orthorhombic 222	$a_1 + a_2 \cos(2\chi)$	0	0
orthorhombic $mm2$	0	$\sin \chi$	$[a_{10} + a_{11} \cos(2\chi)] \sin \chi$
monoclinic 2	$a_1 + a_2 \cos(2\chi) + a_3 \sin(2\chi)$	0	0
monoclinic m	$a_1 + a_2 \cos(2\chi) + a_3 \sin(2\chi)$	0	0
triclinic 1	$a_1 + a_2 \cos(2\chi) + a_3 \sin(2\chi)$	$a_8 \cos \chi + a_9 \sin \chi$	$[a_{10} + a_{11} \cos(2\chi)] \sin \chi + a_{15} \cos \chi + a_{16} \cos(3\chi)$